sustainability

MDPI

Article

Steel-Concrete Composite Beams with Precast Hollow-Core Slabs: A Sustainable Solution

Felipe Piana Vendramell Ferreira [1], Konstantinos Daniel Tsavdaridis [2,*], Carlos Humberto Martins [3] and Silvana De Nardin [1]

[1] Department of Civil Engineering, Federal University of São Carlos, 13565-905 São Carlos, São Paulo, Brazil; ferreirafpv@gmail.com (F.P.V.F.); snardin@ufscar.br (S.D.N.)
[2] School of Civil Engineering, Faculty of Engineering and Physical Sciences, University of Leeds, Leeds LS2 9JT, UK
[3] Department of Civil Engineering, State University of Maringá, 87020-900 Maringá, Paraná, Brazil; chmartins@uem.br
* Correspondence: k.tsavdaridis@leeds.ac.uk; Tel.: +44(0)-113-343-2299

Abstract: Industrialization of construction makes building operation more environmental friendly and sustainable. This change is necessary as it is an industry that demands large consumption of water and energy, as well as being responsible for the disposal of a high volume of waste. However, the transformation of the construction sector is a big challenge worldwide. It is also well known that the largest proportion of the material used in multistory buildings, and thus its carbon impact, is attributed to their slabs being the main contributor of weight. Steel-Concrete composite beams with precast hollow-core slabs (PCHCSs) were developed due to their technical and economic benefits, owing to their high strength and concrete self-weight reduction, making this system economical and with lower environmental footprint, thus reducing carbon emissions. Significant research has been carried out on deep hollow-core slabs due to the need to overcome larger spans that resist high loads. The publication SCI P401, in accordance with Eurocode 4, is however limited to hollow-core slabs with depths from 150 to 250 mm, with or without a concrete topping. This paper aims to investigate hollow-core slabs with a concrete topping to understand their effect on the flexural behavior of Steel-Concrete composite beams, considering the hollow-core-slab depth is greater than the SCI P401 recommendation. Consequently, 150 mm and 265 mm hollow-core units with a concrete topping were considered to assess the increase of the hollow core unit depth. A comprehensive computational parametric study was conducted by varying the in situ infill concrete strength, the transverse reinforcement rate, the shear connector spacing, and the cross-section of steel. Both full and partial interaction models were examined, and in some cases similar resistances were obtained, meaning that the same strength can be obtained for a smaller number of shear studs, i.e., less energy consumption, thus a reduction in the embodied energy. The calculation procedure, according to Eurocode 4 was in favor of safety for the partial-interaction hypothesis.

Keywords: composite beams; hollow-core slabs; sustainable; finite element analyses

Citation: Ferreira, F.P.V.; Tsavdaridis, K.D.; Martins, C.H.; De Nardin, S. Steel-Concrete Composite Beams with Precast Hollow-Core Slabs: A Sustainable Solution. *Sustainability* **2021**, *13*, 4230. https://doi.org/10.3390/su13084230

Academic Editor: Jorge de Brito

Received: 17 March 2021
Accepted: 7 April 2021
Published: 10 April 2021

1. Introduction

Researchers have been studying the impact that civil construction causes on the environment. In this context, a concept that has been studied is embodied energy in materials of buildings [1]. In Whitworth and Tsavdaridis [2,3], optimization studies were presented in Steel-Concrete composite beams with the objective of presenting sustainable structural designs by minimizing the embodied energy. The study showed that it is possible to reduce the embodied energy of these structural systems, considering the design recommendations of Eurocode 4 [4].

Conventional Steel-Concrete composite beams have a concrete slab that is placed at the upper flange of the downstand steel profile. In this context, three types of slabs can be

used: solid, composite or precast hollow-core slabs (PCHCSs). In composite beams with PCHCSs, a cast in situ concrete topping is usually made to provide a smooth and uniform finish [5]. The concrete topping can increase the strength and stiffness of the structural system [6,7]. Other factors influence the strength of PCHCSs, such as the intensity of the actual prestress, the prestress transmission length, the depth of the slab, and filled cores [8]. PCHCSs are widely used in countries with cold climates in the construction of residential or industrial buildings due to their fast installation. In Albero et al. [9], the estimate of the number of PCHCS floors installed in Europe was estimated to be close to 1 billion square meters. The use of PCHCSs offers advantages; e.g., large spans, speed of construction, and reduced construction costs [5,10–14]. In the European Union, according to Ahmed and Tsavdaridis [15], construction and building are responsible for about 40% of environmental impact. In Dong et al. [16], the precast and cast in situ construction methods were compared using a case study. The authors concluded that the precast construction could lead to a 10% carbon reduction for one cubic meter of concrete. The PCHCS is an industrialized structural element that consumes less energy when constructed in-house in comparison to in situ, and with a minimum waste of concrete, and thus with an overall lower carbon footprint. In terms of sustainability, the PCHCS is a structural element that contributes not only to the speed of construction, but also to the significant reduction of CO_2 emissions due to the lower consumption of concrete.

The present study aims to examine the flexural behavior of Steel-Concrete composite beams with PCHCSs and a concrete topping, considering a hollow core unit (HCU) depth greater than the SCI P401 recommendation. The finite element (geometrical nonlinear analysis) model was developed based on tests [17,18]. The results were compared with the SCI P401 procedure [19], and thus analytical models of shear-stud resistance capacity were employed [19,20].

2. Background

Lam [17] and Lam et al. [21] presented flexural tests on Steel-Concrete composite beams with PCHCSs. A four-point bending was considered. In these studies, the concrete topping was not considered. The experimental results showed a sudden failure due to the shear studs rupturing and the concrete cracking, resulting in a loss of stiffness. Lam et al. [22] complemented the previous studies and carried out a parametric study in which they observed that with an increase in the depth of PCHCSs (150 mm to 200–250 mm), there was an increase in the ultimate strength. However, the slab could fail due to excessive cracking. Ellobody and Lam [23] investigated the shear studs and the gap while considering the flexural behavior. The authors concluded that the shear-stud resistance increased with the increase of the gap, and the in situ infill concrete strength influenced the strength of the shear studs. In 2003, SCI P287 [24] was published; it is a design criteria for composite beams with PCHCSs [17]. This publication was subsequently updated to SCI P401 [19]. The document gathers recommendations of minimum dimensions, such as arrangement of the shear studs and transverse reinforcement. However, some limitations were observed, such as application only for 150–250 mm HCU depths; 12 mm or 16 mm transverse reinforcement diameters are recommended for composite construction. For partial shear connection, 16 mm diameter bars should be provided; for HCUs up to 260 mm, 16 mm diameter bars should be considered, spaced at 200–350 mm. For full interaction, if the plastic neutral axis (PNA) lies within the slab, the interaction degree must be reduced, or the size of the steel profile increased. A technical report (COPPETEC, PEC-18541/2016), which was presented by Batista and Landesmann [18], described tests on composite beams with PCHCSs and concrete topping. According to the authors, at the ultimate strength, the loss of stiffness was due to excessive cracking. In Ferreira et al. [25], a parametric study was presented, considering PCHCSs with 150 mm of depth and 50 mm of concrete topping. In this study, the presence of the concrete topping increased the strength of the composite beams by at least 7%. As observed, few studies have investigated the behavior of Steel-Concrete composite beams with PCHCSs [26]. Tawadrous and Morcous [4] and

El-Sayed et al. [5] showed that, due to the successful use of PCHCSs, deeper HCUs were developed to resist higher loads and to support longer spans. In this scenario, some researchers carried out tests to investigate the behavior of deeper PCHCSs [12,13,27–32]. However, these investigations did not consider composite behavior, i.e., Steel-Concrete composite beams.

3. Numerical Model: Validation Study

In this section, the methodology of the validation study is described. The ABAQUS software [33] was used. Three types of Steel-Concrete composite beams were modeled, considering symmetry:

1. 150 mm of HCU depth with a chamfered end (Figure 1a);
2. 150 mm of HCU depth and 50 mm of concrete topping with a squared end (Figure 1b);
3. 265 mm of HCU depth and 50 mm of concrete topping with a squared end (Figure 1c).

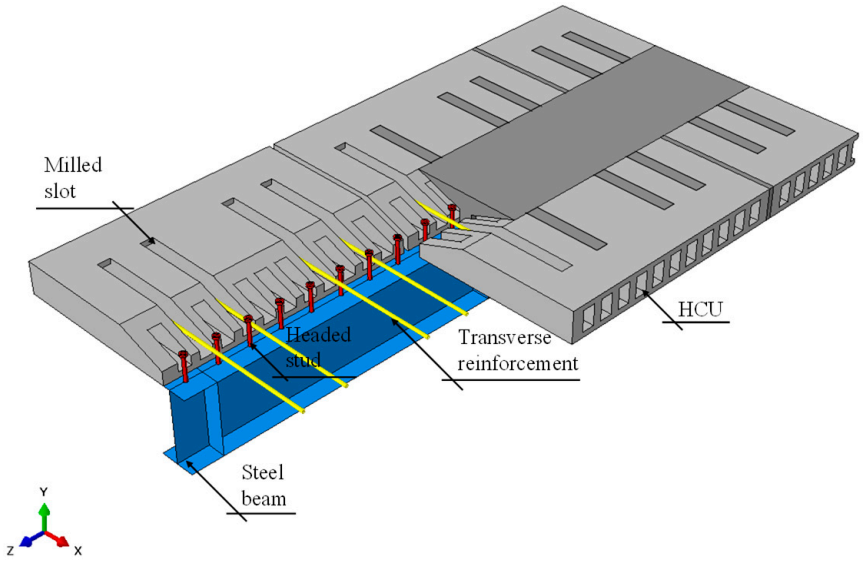

(**a**)

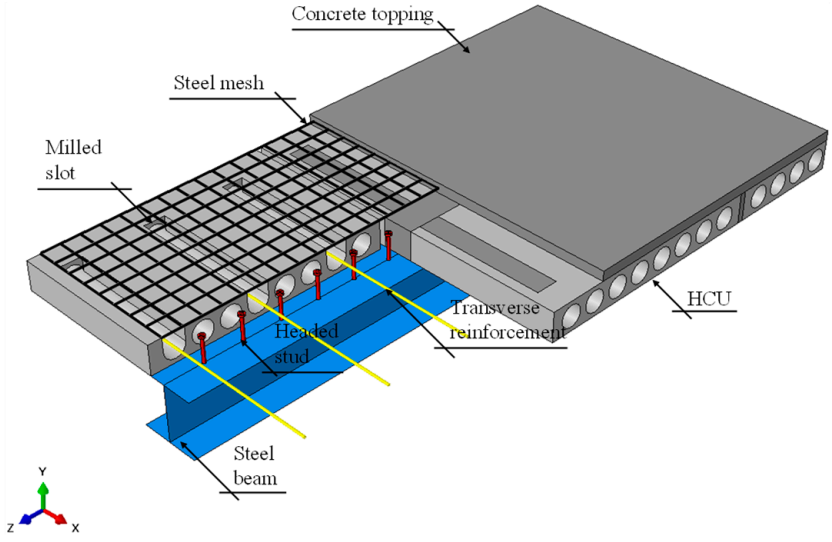

(**b**)

Figure 1. *Cont.*

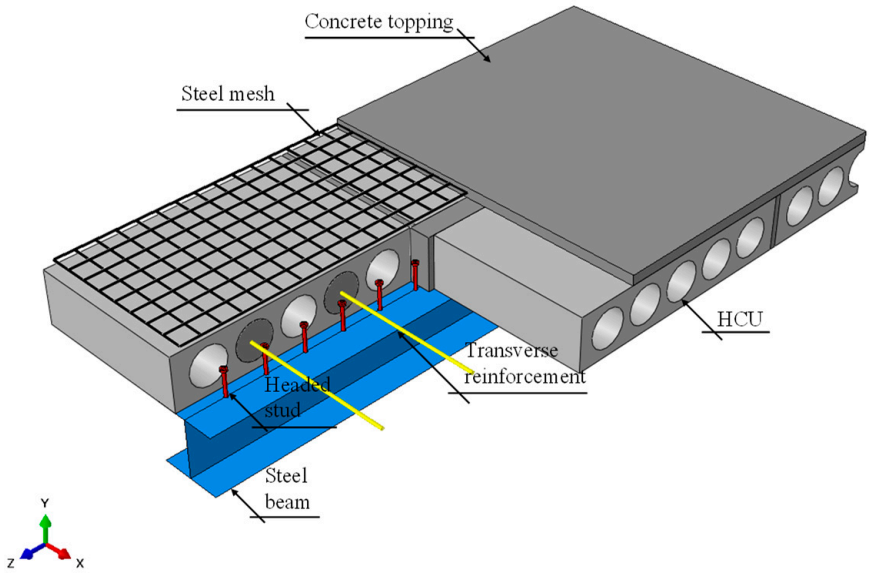

(**c**)

Figure 1. Parts of Steel-Concrete composite beams with a hollow core slab: (**a**) 150 mm of hollow-core-slab depth with a chamfered end; (**b**) 150 mm of hollow-core-slab depth and 50 mm of concrete topping with a squared end; (**c**) 265 mm of hollow-core-slab depth and 50 mm of concrete topping with a squared end.

Geometrical nonlinear analyses were processed using the Static Riks method. This method was previously used in [25,34–40] and is based on the arc-length method. Residual stresses were not considered. These stresses do not influence the ultimate strength of composite beams subjected to only positive moments. The residual stresses increase the effects of the negative moment [41,42].

3.1. Tests

The numerical models were calibrated considering tests on Steel-Concrete composite beams with PCHCSs, at 150 mm and 265 mm of depth, and with or without a concrete topping. Figure 2 and Table 1 show the details of the tests [18,43], in which d is the steel-beam depth, b_f is the steel-flange width, t_f is the steel-flange thickness, t_w is the steel-web thickness, b is the effective slab width, g is the gap, h_c is the depth of the HCU, c is the concrete-topping thickness, L_e is the distance between the end of the beam and the support, L_p is the distance between the load application point and the support, L_b is the unrestrained length, φ is the diameter of the transverse reinforcement, $f_{y,f}$ is the yield strength of the flange, $f_{y,w}$ is the yield strength of the web, $f_{y,s}$ is the transverse reinforcement yield strength, $f_{c,HCU}$ is the HCU compressive strength, and $f_{c,in}$ is the in situ infill compressive strength.

Table 1. Details of specimens (in mm and MPa).

Model	d	b_f	t_f	t_w	b	g	h_c	c	L_e	L_p	L_b	φ	$f_{y,f}$	$f_{y,w}$	$f_{y,s}$	$f_{c,HCU}$	$f_{c,in}$
CB1	355	171.5	11.5	7.4	1665	65	150	-	150	1500	5700	16	310	355	585	50 [a]	32 [a]
CB2	355	171.5	11.5	7.4	1665	65	150	-	150	1500	5700	8	310	355	473	50 [a]	26 [a]
CB3	299	306	11	11	1756	156	150	50	185	1915	5830	12.5	345	345	500	45 [b]	30 [b]
CB4	299	306	11	11	1756	106	265	50	185	1915	5830	12.5	345	345	500	45 [b]	30 [b]

[a] Cubic resistance; [b] cylindric resistance.

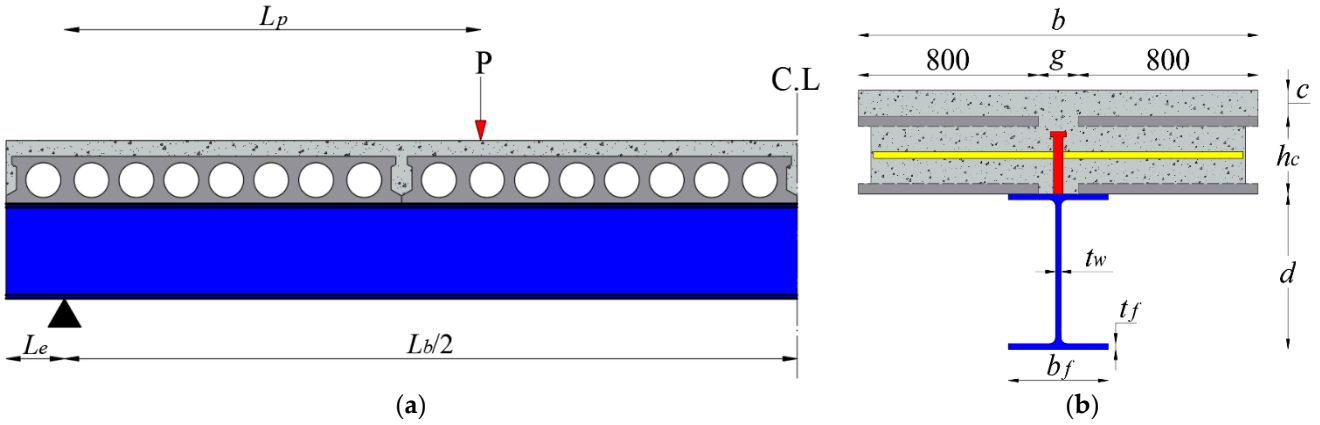

Figure 2. Geometric details of tests (in mm): (**a**) lateral view; (**b**) section.

The shear-stud dimensions were 19 × 125 mm^2 (CB1 and CB2) and 19 × 135 mm^2 (CB3 and CB4). The shear-stud spacing of the CB1 and CB2 models was 150 mm. For models CB3 and CB4, the spacing between the shear studs was 200 mm.

3.2. Materials

The concrete-damage plasticity (CDP) [44–46] model was used. This model is based on the plastic theory, and can be used to describe the irreversible damage that occurs during the fracture process [33], such as cracking and crushing. The concrete-damage plasticity model makes use of the yield function of Lubliner et al. [45], with modifications proposed by Lee and Fenves [46]. Concrete, as a brittle material, undergoes considerable volume change called dilatancy [47], which is caused by inelastic strains. The flow rule followed the Drucker–Prager model. The concrete-damage plasticity model can be regularized using viscoplasticity. The regularization of Duvaut-Lions [48] was used. The input parameters for defining the plastic behavior are presented in Table 2, in which ψ is the dilation angle, ξ is the eccentricity, σ_{b0} is the initial equibiaxial compressive yield stress, σ_{c0} is the initial uniaxial compressive yield stress, K_c is the ratio of the second stress invariant on the tensile meridian to that on the compressive meridian, and μ is the viscosity parameter.

Table 2. Concrete Damage Plasticity input parameters [25,38,40].

Parameter	Value	Ref.
Ψ (°) (In situ concrete)	40	[47,49]
Ψ (°) (HCU concrete)	28	[28]
ξ	0.1 (default)	[28,33,47,49]
σ_{b0}/σ_{c0}	1.16 (default)	[28,33,47,49]
K_c	2/3 (default)	[28,33,47,49]
μ (s^{-1})	0.001	-

The concrete model of Carreira and Chu [50,51] was used for both compression and tension Equations (1)–(3). For steel, the perfect elasto-plastic behavior was considered.

$$\frac{\sigma}{f_c} = \frac{\beta_c(\varepsilon/\varepsilon_c)}{\beta_c - 1 + (\varepsilon/\varepsilon_c)^{\beta_c}} \quad (1)$$

$$\frac{\sigma}{f_t} = \frac{\beta_c(\varepsilon/\varepsilon_t)}{\beta_c - 1 + (\varepsilon/\varepsilon_t)^{\beta_c}} \quad (2)$$

$$\beta_c = \left(\frac{f_c}{32.4}\right)^3 + 1.55(\text{MPa}) \quad (3)$$

where ε_c is the strain corresponding to concrete compressive strength, ε_t is the strain corresponding to concrete tensile strength, f_c is the compressive concrete strength, f_t is the concrete tensile strength, and β_c is the stress–strain relationship form factor of concrete in compression.

3.3. Interaction

Figure 3 shows the pairs of interactions. The tie constraint technique allowed us to simulate the perfect bond between the contact surfaces. The contacts between the concrete and the transverse reinforcements were made through the embedded region [33]. The normal/tangential behavior was considered between the steel beam and PCHCS, the steel beam and gap, the actuator and concrete topping, and the shear stud and gap. The shear studs were located in the gap, using the same technique presented in [52]. The friction coefficient was based on the Coulomb friction model. The literature reports some values of the friction coefficient [53–55]. Friction coefficients of 0.2 and 0.3 were adopted for the gap and headed stud and the steel beam and slab interfaces, respectively [55].

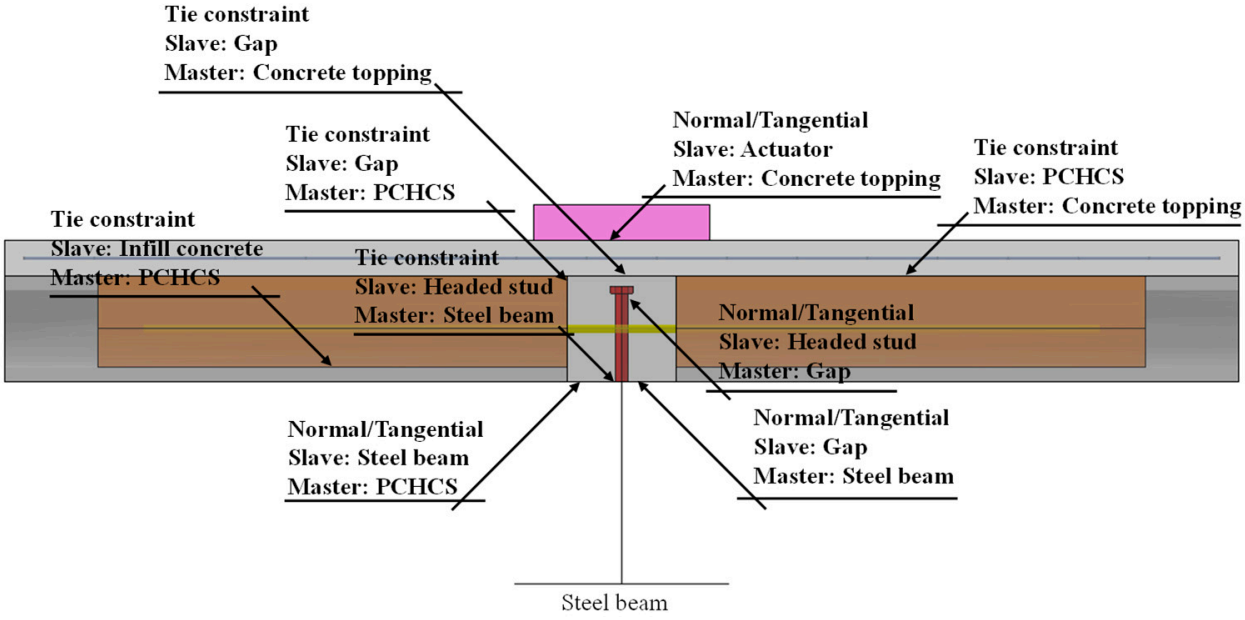

Figure 3. Surface-to-surface interactions.

3.4. Boundary Conditions

The boundary conditions (Figure 4) were applied considering the symmetry at midspan ($U_z = UR_x = UR_y = 0$) [25,37–40]. The vertical displacement was restrained at the supports ($U_y = 0$) and the lateral displacement at the ends of the slab ($U_x = 0$). Displacement control was used. The difficulties with softening materials can be avoided by applying a simple form of displacement control [56,57]. The disadvantages in displacement control are related to the selection of the appropriate displacement variable [58]. Thus, the variable selected for the stopping criterion was the midspan vertical displacement.

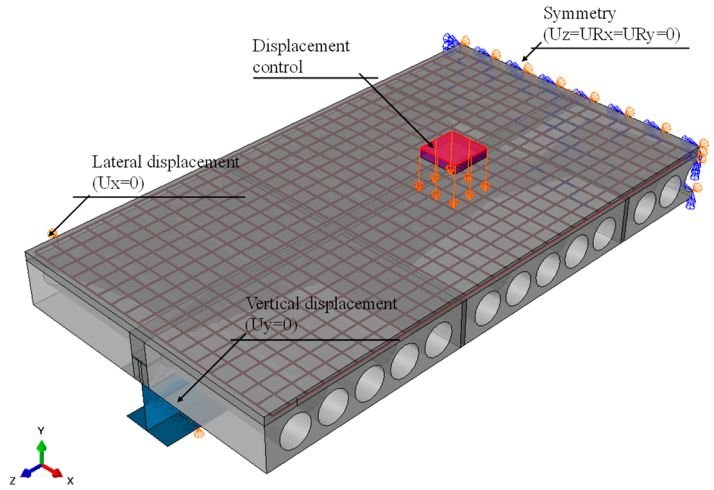

Figure 4. Boundary conditions of the CB3 model.

3.5. Discretization

The discretization of the elements is shown in Figure 5. The dimension values of the elements were adopted according to the literature [28,53,54], and with respect to the master and slave surfaces. The S4R element was a quadrilateral element with four nodes. This element had reduced integration. According to the ABAQUS, Dassault Systèmes, software [33], the C3D8R element had eight nodes, reduced integration, supported plastic analysis with large deformations, and allowed the visualization of the crack in the CDP model. The T3D2 element had 2-node linear displacement.

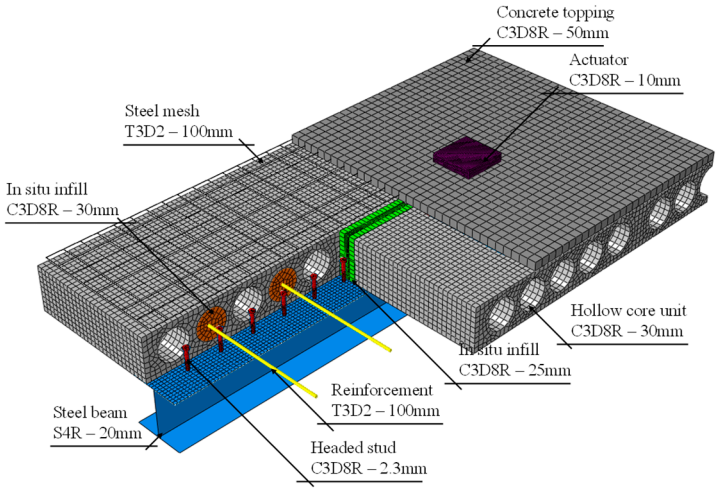

Figure 5. Discretization.

3.6. Results

The results are presented in Figure 6 and Table 3, in which M_{FE} is the bending moment of finite element model, M_{Test} is the bending moment of experimental tests, δ_{FE} is the midspan vertical displacement of the finite element models, and δ_{Test} is the mid-pan vertical displacement of the tests. It was possible to observe the yielding at the lower flange, and in the CB1 and CB2 models, the cracking was observed in the lower part of the PCHCSs, according to Lam [17]. The behaviors of the CB3 and CB4 models were similar to those presented in Batista and Landesmann [18]; that is, there was a propagation of cracks that started in the central part of the PCHCS and extended over the entire width.

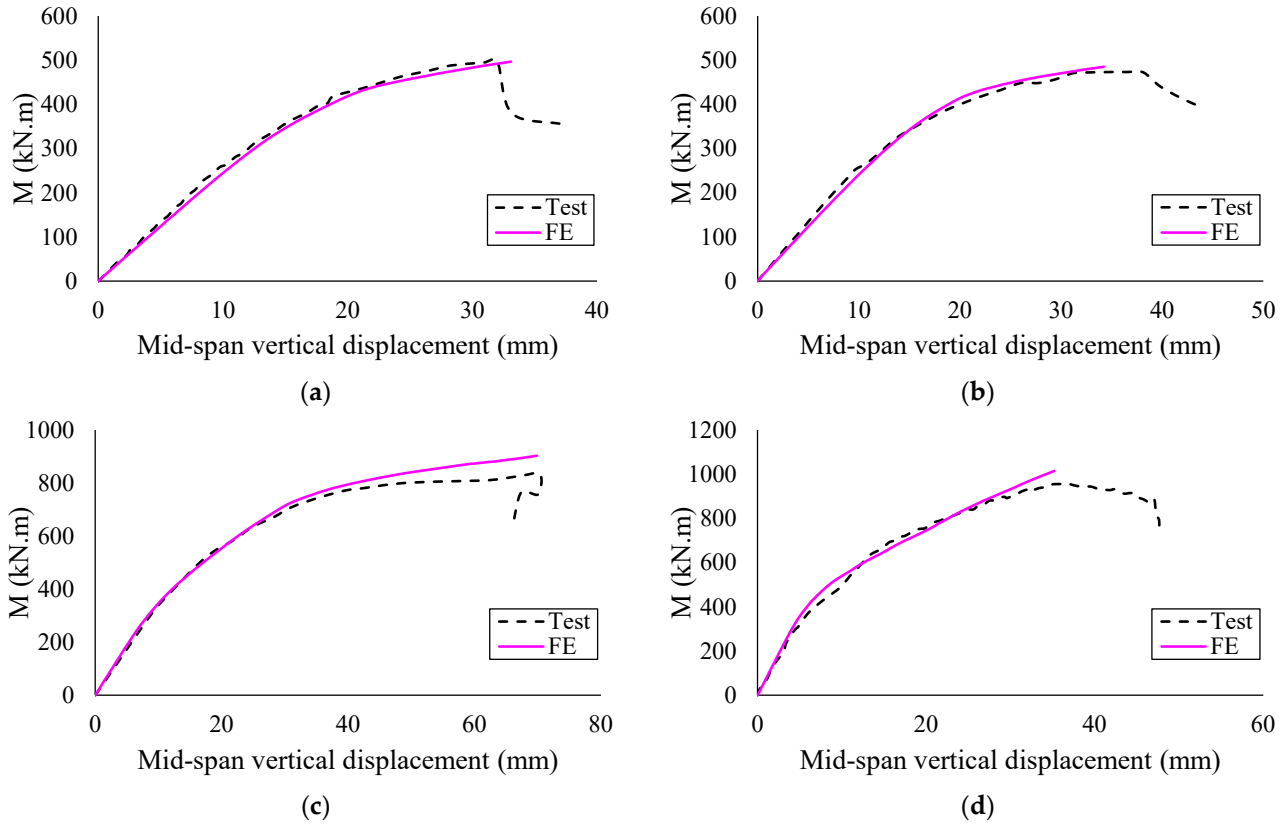

Figure 6. Validation results: (**a**) CB1 model; (**b**) CB2 model; (**c**) CB3 model; and (**d**) CB4 model.

Table 3. Comparison of finite element analyses and tests results.

Model	M_{Test} (kN.m)	δ_{Test} (mm)	M_{FE} (kN.m)	δ_{FE} (mm)	M_{FE}/M_{test}	$\delta_{FE}/\delta_{test}$
CB1	497	32	496	33	1.00	1.03
CB2	474	35	485	34	0.95	0.97
CB3	846	70	895	71	0.95	1.00
CB4	985	37	1015	35	1.03	0.95

4. Numerical Model: Parametric Study

The following were the general considerations for the parametric study:

1. The thickness of the concrete topping was 50 mm;
2. The total transverse reinforcement length was 1000 + g, in mm;
3. A welded steel mesh with 4.2 mm × 100 mm was considered [20,25];
4. LP26 units (Figure 7), with f_c = 40 MPa and g = 70 mm, were considered;
5. For the steel beam, the ASTM A572 Gr.50 steel was adopted (f_y = 345 MPa). The Young's module and the Poisson's ratio were 200 GPa and 0.3, respectively;
6. The composite beams were simply supported, and subjected to four-point bending. The loads were spaced in $L/4$ from each support. Stiffeners were placed at the support and points of loads;
7. The midspan vertical displacement of a maximum value equal to $L/100$ was adopted as a stopping criterion [25].

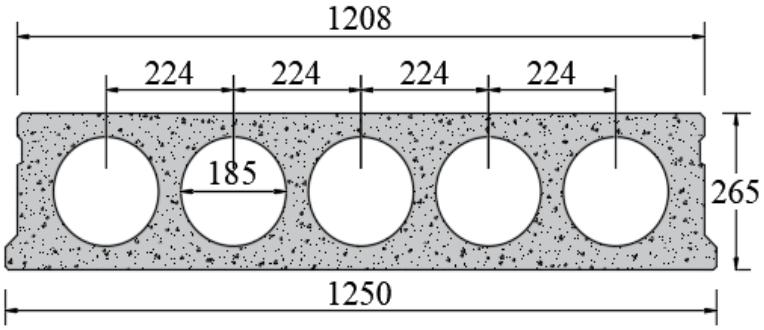

Figure 7. LP26 units (in mm).

The studied parameters are shown in Table 4.

Table 4. Parametric study.

Parameters	Variation
Section	W360x51, W460x74, and W530x72
In situ concrete strength (MPa)	25, 30, and 40
Transverse reinforcement diameter (mm)	10, 12.5, and 16
Shear-stud spacing (mm)	125, 175, and 275

5. Results and Discussion

In this section, the results are discussed, according to the steel cross-sections that were analyzed. At the end of this section, the results are compared with the resistant calculation procedures for Steel-Concrete composite beams, as well as with the results presented in Ferreira et al. [25], considering a 150 mm depth of the PCHCS with concrete topping.

5.1. W360x51 Section

Considering a spacing between shear studs of 120 mm, for the midspan vertical displacement at 15 mm, only the region where the beam was supported reached the yield strength. The maximum von Mises stresses in the lower flange, web, and upper flange were approximately 290 MPa, 260 MPa, and 115 MPa, respectively. When the composite beam reached the ultimate strength, for the midspan vertical displacement at 26 mm, the lower flange and approximately 1/4 of the web depth were in the plastic regime. The yield strength was reached in none of the regions where the shear studs were located. The von Mises stresses in the upper flange were approximately 200 MPa. The ultimate strength was governed by excessive cracking of the PCHCS (Figure 8).

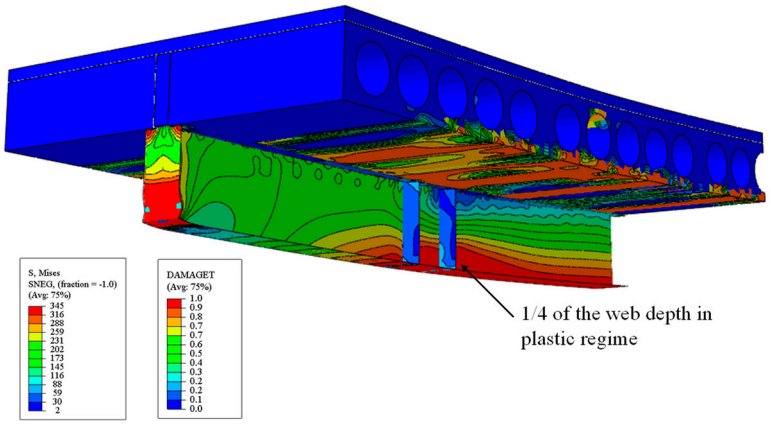

Figure 8. Final configuration for W360x51, f_c = 25 MPa, φ = 10 mm, and 120 mm of spacing.

With the variation of the transverse reinforcement rate and in situ concrete strength, there were no differences in the shear-slip and moment-deflection relationships (Figure 9).

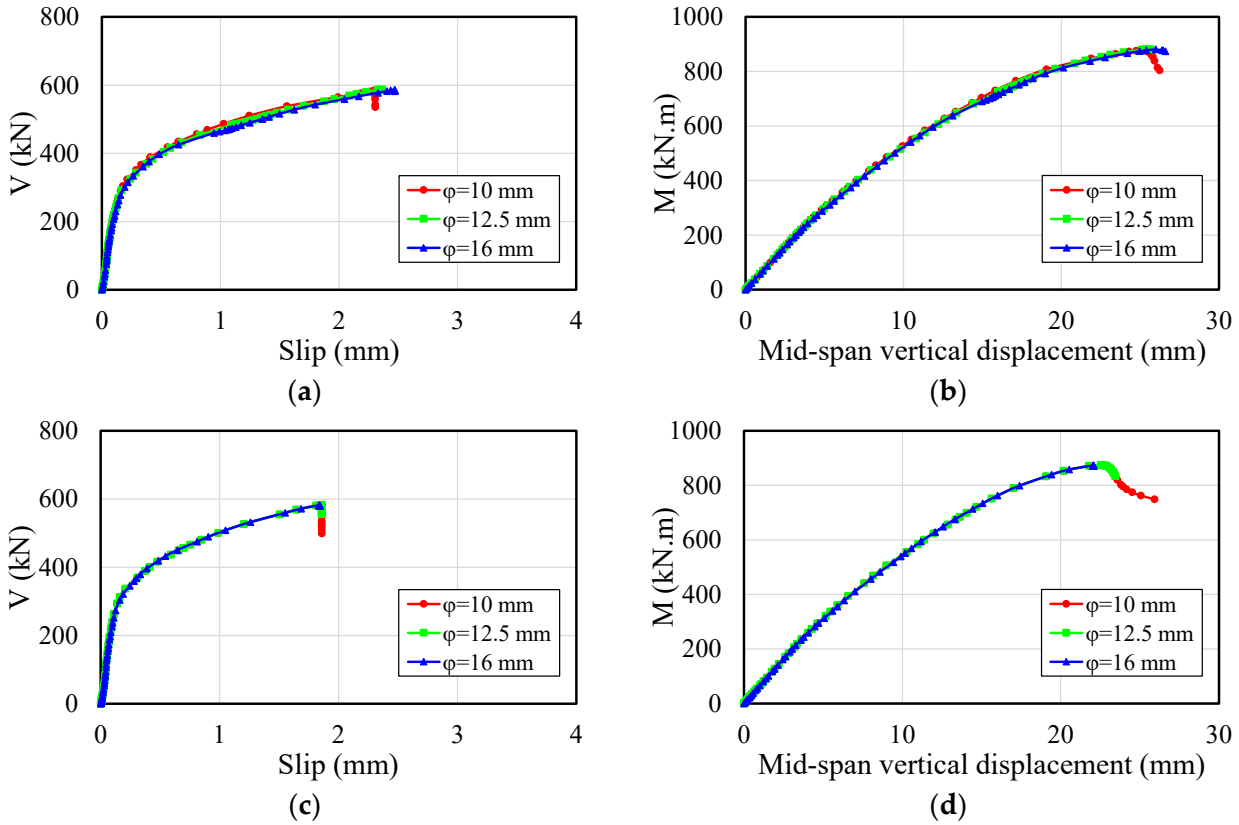

Figure 9. Influence of transverse reinforcement for the W360x51 section with 120 mm of spacing: (**a**) Shear-slip relationship for f_c = 25 MPa; (**b**) moment-deflection relationship for f_c = 25 MPa; (**c**) shear-slip relationship for f_c = 40 MPa; and (**d**) moment-deflection relationship for f_c = 40 MPa.

This can be explained as a function of the depth and area of the steel cross-section in relation to the depth and effective area of the PCHCS and concrete topping. Upon reaching the ultimate strength, as shown in Figure 8, the neutral plastic axis (NPA) was in the concrete topping, a factor that generates excessive tensile stresses in the PCHCS. This can be concluded since in the final configuration, the upper part of the PCHCS, which was in the region of pure bending, was damaged. Another important observation was the fragile behavior of the composite beams, since the slip values at the steel-concrete interface were less than 6 mm, a parameter that Eurocode 4 [4] considers to characterize the ductile behavior (Figure 9). Due to this fragile behavior, with the variation of parameters, such as transverse reinforcement rate and in situ concrete strength, there were no significant differences in terms of stresses, both in the shear studs and in the transversal reinforcement, considering the ultimate strength. Some examples are illustrated in Figure 10. For the models with f_c = 25 MPa, it was observed that the smaller the transverse reinforcement diameter, the lower the von Mises stresses in the shear stud. For f_c = 25 MPa, the von Mises stresses in the shear studs showed a variation of only 6 MPa. On the other hand, for f_c = 40 MPa, there were no variations between the von Mises stresses in the shear studs with the variation of the transverse reinforcement diameter. The observations for f_c = 30 MPa were similar.

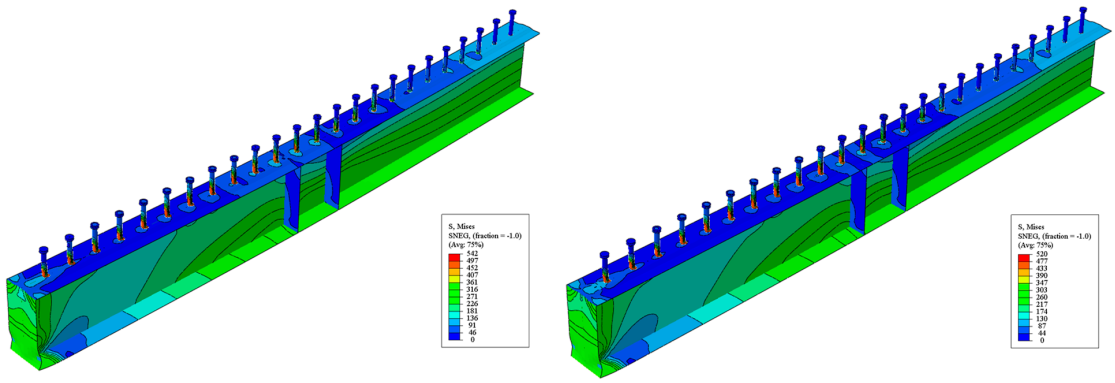

(**a**) (**b**)

Figure 10. The von Mises stresses in headed studs for the W360x51 section and spacing of 120 mm: (**a**) f_c = 25 MPa and φ = 10 mm; (**b**) f_c = 40 MPa and φ = 16 mm.

On the other hand, for the shear-stud spacing at 175 mm and 225 mm, for the midspan vertical displacement at 15 mm, the behavior was similar to the models with 120 mm of spacing. However, at the ultimate strength, the midspan vertical displacements were greater than in the previous situation, with the maximum value equal to 36 mm, considering φ = 16 mm, f_c = 40 MPa, and 175 mm of spacing. For the situation in which the spacing was 225 mm, the midspan vertical displacement reached 42 mm, considering φ = 10 mm and f_c = 25 MPa. Regarding the ultimate strength, the composite beams with shear-stud spacing of 175 mm and 225 mm made better use of the steel section; that is, approximately half the web depth reached plastification (Figure 11). Then, the greater the spacing between the shear studs, the better the use of the steel section.

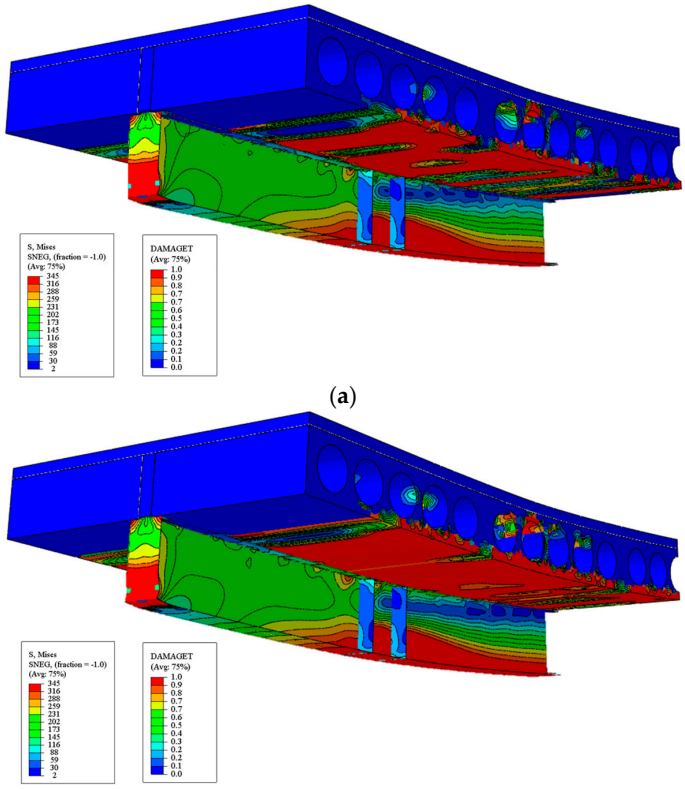

(**a**)

(**b**)

Figure 11. Final configuration for the W360x51 section: (**a**) 175 mm of spacing, f_c = 40 MPa, and φ = 16 mm; and (**b**) 225 mm of spacing, f_c = 25 MPa, and φ = 10 mm.

The variation in both the transverse reinforcement rate (Figures 12 and 13) and the in situ concrete strength showed significant differences in the shear-slip and moment-deflection relationships.

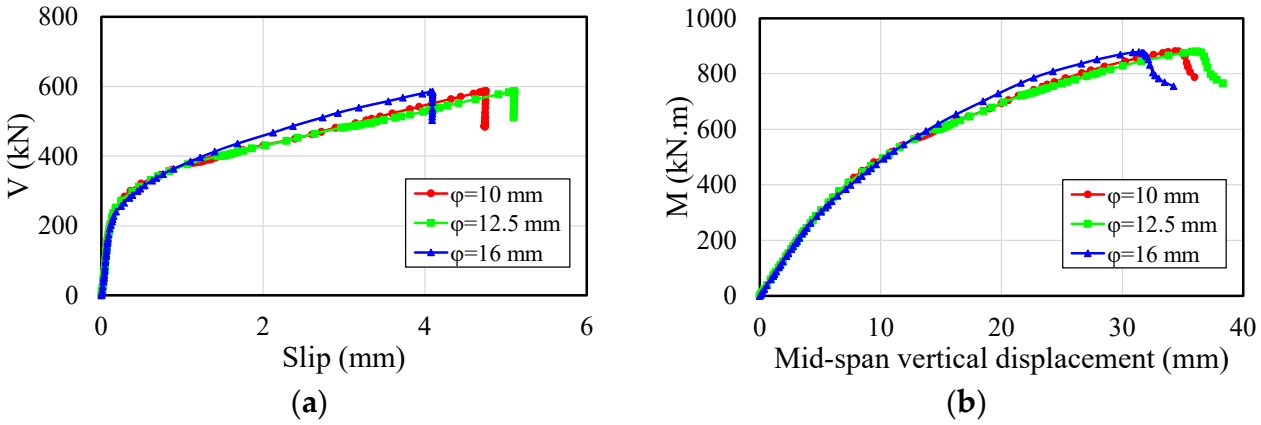

Figure 12. Influence of transverse reinforcement for the W360x51 section, f_c = 40 MPa and175 mm of spacing: (**a**) shear-slip relationship; and (**b**) moment-deflection relationship.

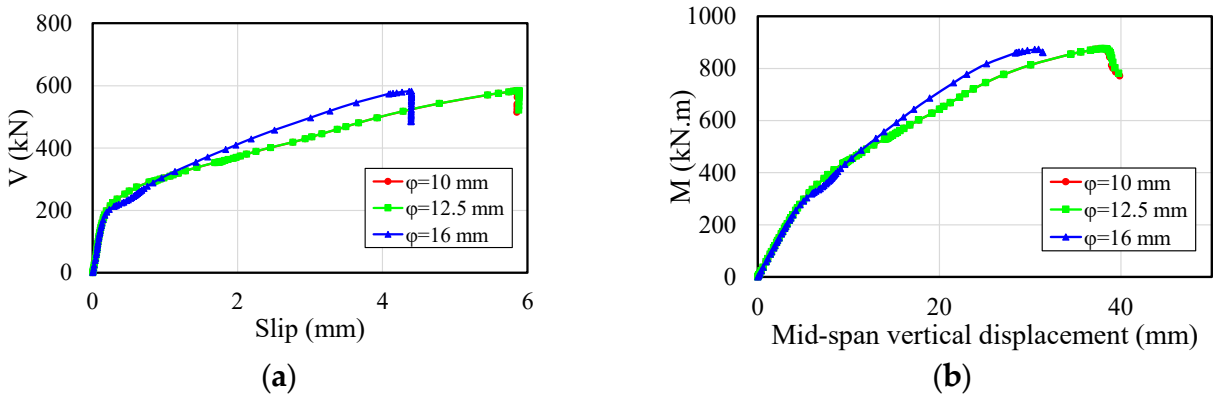

Figure 13. Influence of transverse reinforcement for the W360x51 section, f_c = 40 MPa and 225 mm of spacing: (**a**) shear-slip relationship; and (**b**) moment-deflection relationship.

As shown in the illustrations, even with the variation of the transverse reinforcement rate and in situ concrete strength, the initial stiffnesses of the composite beams modeled were similar, showing that the differences of these relations were significant in the non-linear branch. Although the ultimate moment had an approximate value for the models illustrated (φ = 10 mm, φ = 12.5 mm, and φ = 16 mm), the models with φ = 10 mm and φ = 12.5 mm showed similar behavior in the shear-slip and moment-deflection relationships, and were different from the model with φ = 16 mm (Figures 12 and 13). According to Lam et al. [22], with the increase in the transverse reinforcement rate, the flexural strength capacity increases, but reduces the ductility, leading to fragile rupture.

Another important observation was that in no model presented for the W360x51 section did the composite beams show ductile behavior. Thus, it was possible to conclude that in all models analyzed for W360x51 section, the ultimate strength was characterized as fragile. In most observations for both 175 mm and 225 mm of spacing, the von Mises stresses in the shear studs were less than the models with 120 mm of spacing. For example, for f_c = 25 MPa, considering the 175 mm and 225 mm models, the von Mises stresses in the shear studs were lower than the model with 120 mm of spacing. A similar situation occurred for f_c = 30 MPa. On the other hand, for f_c = 40 MPa, there were models in which the von Mises stresses in the shear studs, considering 175 mm and 225 mm of spacings,

were greater than the model with 120 mm of spacing. This was observed specifically for transversal-reinforcement diameters equal to 10 mm and 12.5 mm.

5.2. W460x74 Section

Considering 120 mm of spacing between the shear studs, for the midspan vertical displacement at 15 mm, only the region in which the beam was supported reached the yield strength. The von Mises stresses in the lower flange, web, and upper flange were 290 MPa, 290 MPa, and 120 MPa, respectively. When the composite beam reached its ultimate strength, the upper flange and approximately 1/4 of the web depth were in the plastic regime. The von Mises stresses in the upper flange were 230 MPa. The ultimate strength was governed by excessive cracking of the PCHCS (Figure 14).

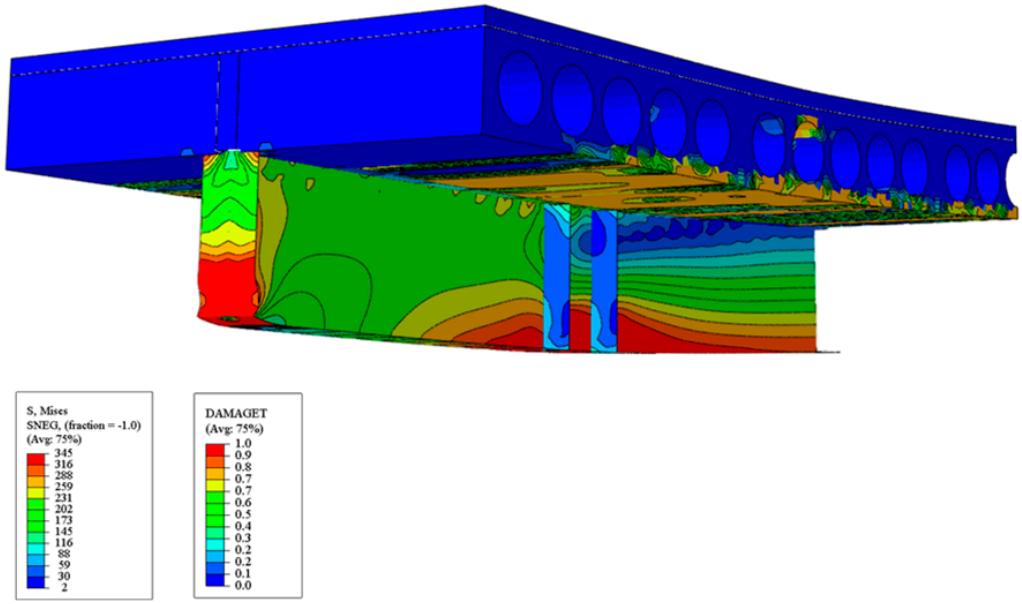

Figure 14. Final configuration for the W460x74 section, f_c = 25 MPa, φ = 10 mm, and 120 mm of spacing.

With the transverse reinforcement rate variation and in situ concrete strength, there were no differences in the shear-slip and moment-deflection relationships (Figure 15).

As noted, there were no significant differences in the behavior of these analyzed composite beams, because the ultimate strength was achieved by excessive cracking of the PCHCS, a situation analogous to the W360x51 section. Another important observation was the fragile behavior of the composite beams, a situation similar to the W360x51 section. Due to this fragile behavior, with the variation of the parameters such as transverse reinforcement rate and in situ concrete strength, there were small differences in the magnitude of the von Mises stresses, specifically in the shear studs. Some examples are illustrated in Figure 16.

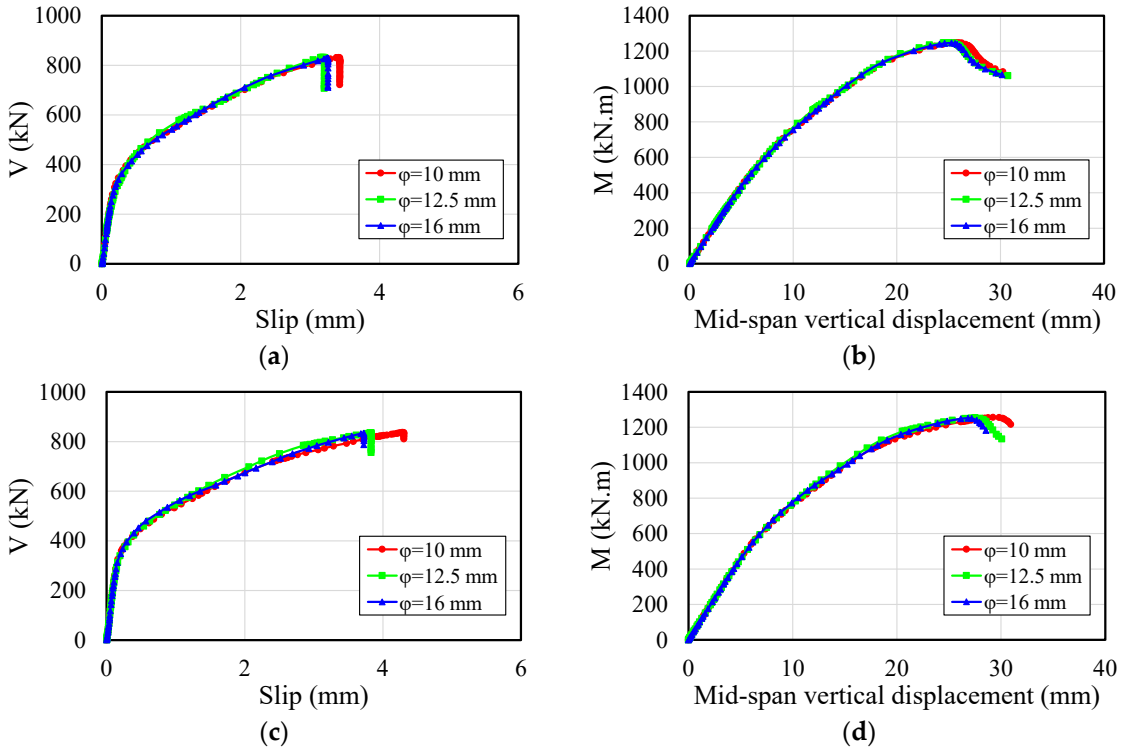

Figure 15. Influence of transverse reinforcement for the W460x74 section and 120 mm of spacing: (**a**) shear-slip relationship for f_c = 25 MPa; (**b**) moment-deflection relationship for f_c = 25 MPa; (**c**) shear-slip relationship for f_c = 40 MPa; and (**d**) moment-deflection relationship for f_c = 40 MPa.

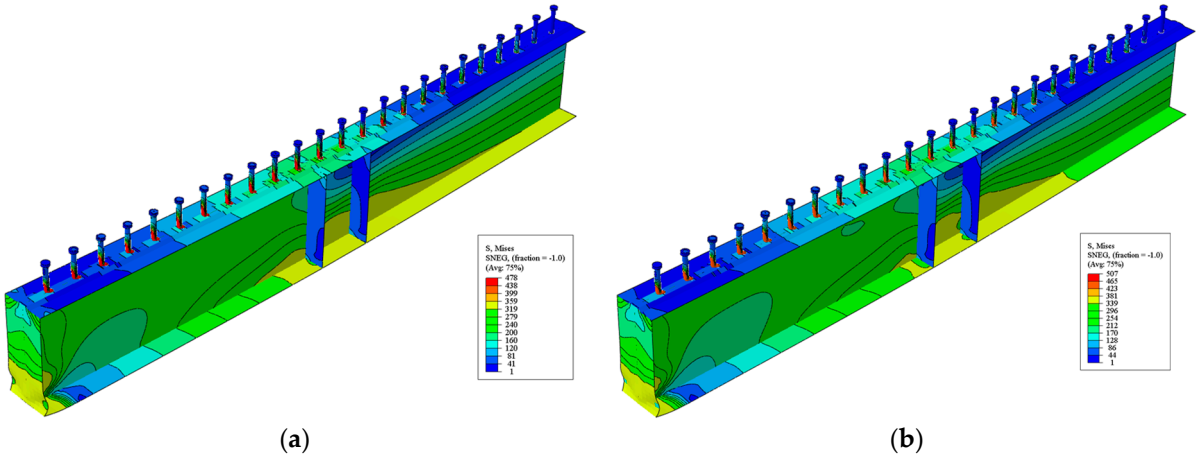

Figure 16. The von Mises stresses in headed studs for the W460x74 section and 120 mm of spacing: (**a**) f_c = 25 MPa and φ = 10 mm; and (**b**) f_c = 40 MPa and φ = 16 mm.

For the f_c = 25 MPa models, the smaller the transverse reinforcement diameter, the lower the von Mises stresses in the shear studs. There was no variation in the stresses in the shear studs for f_c = 25 MPa. A similar situation occurred for f_c = 30 MPa models. For the f_c = 40 MPa models, the von Mises stresses in the shear studs varied with the variation of the transverse reinforcement diameter. Unlike the f_c = 25 MPa models, the smaller the transverse reinforcement diameter, the greater the von Mises stresses in the shear studs. This variation reached approximately 20 MPa between φ = 10 mm and φ = 16 mm.

Considering the models with 175 mm and 225 mm of spacing, it was possible to observe two different situations. In relation to the 175 mm of spacing, for the midspan

vertical displacement at 15 mm, the yield strength was not reached in any region of the steel profile. The maximum von Mises stresses in the lower flange, web, and upper flange were 290 MPa, 290 MPa, and 120 MPa, respectively. When the composite beams reached the ultimate strength, only part of the lower flange was in the plastic regime (Figure 17a). For 225 mm of spacing between shear studs, the ultimate strength was characterized with the lower flange, half the web depth, and part of the upper flange, which were in the region of the loading application point, in the plastic regime (Figure 17b). This was the model in which the composite action took advantage of the strength of the steel profile.

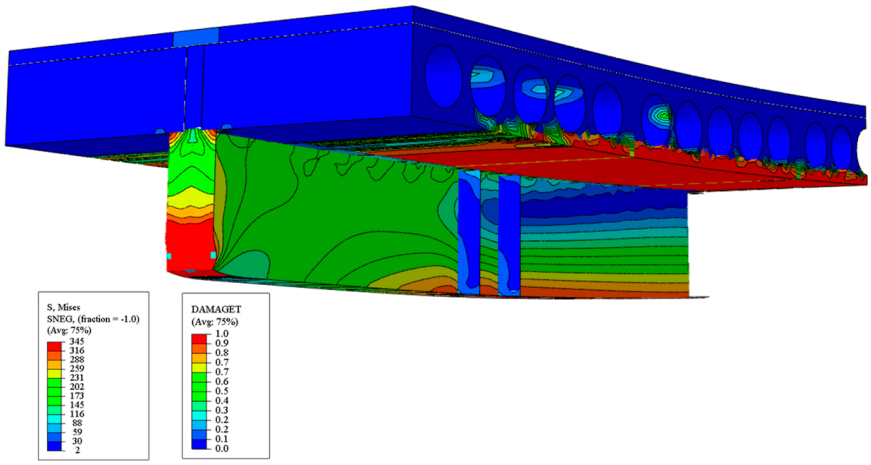

(**a**)

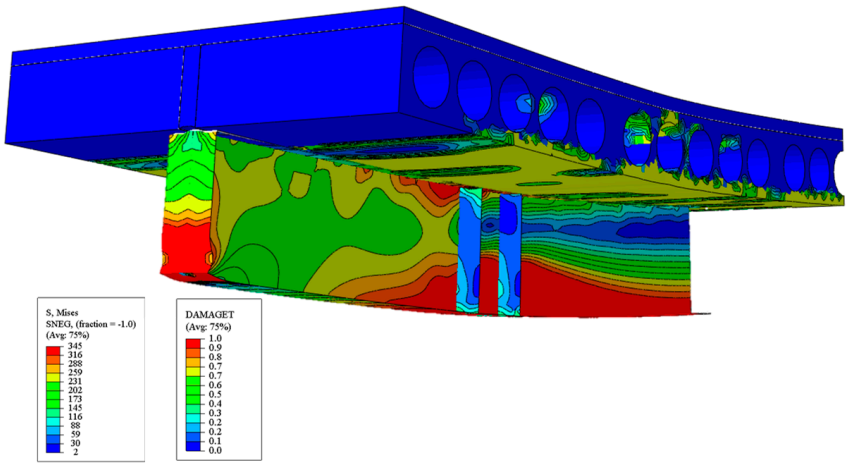

(**b**)

Figure 17. Final configuration for the W460x74 section: (**a**) 175 mm of spacing, f_c = 40 MPa, and φ = 10 mm; and (**b**) 225 mm of spacing, f_c = 40 MPa, and φ = 16 mm.

The variation in both the transverse reinforcement rate and the in situ concrete strength (Figures 18 and 19) showed significant differences in the shear-slip and moment-deflection relationships.

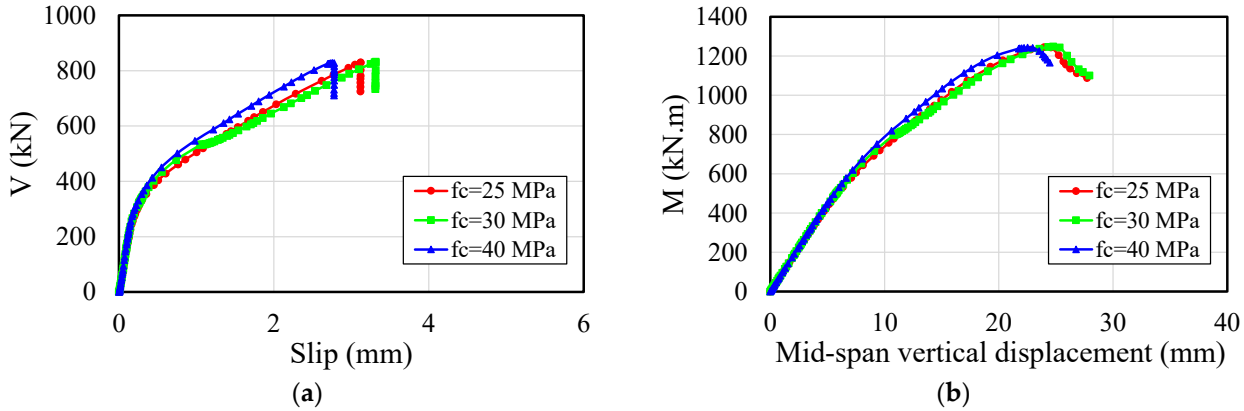

Figure 18. Influence of in situ concrete strength for the W460x74 section, φ = 12.5 mm and 175 mm of spacing: (**a**) shear-slip relationship; and (**b**) moment-deflection relationship.

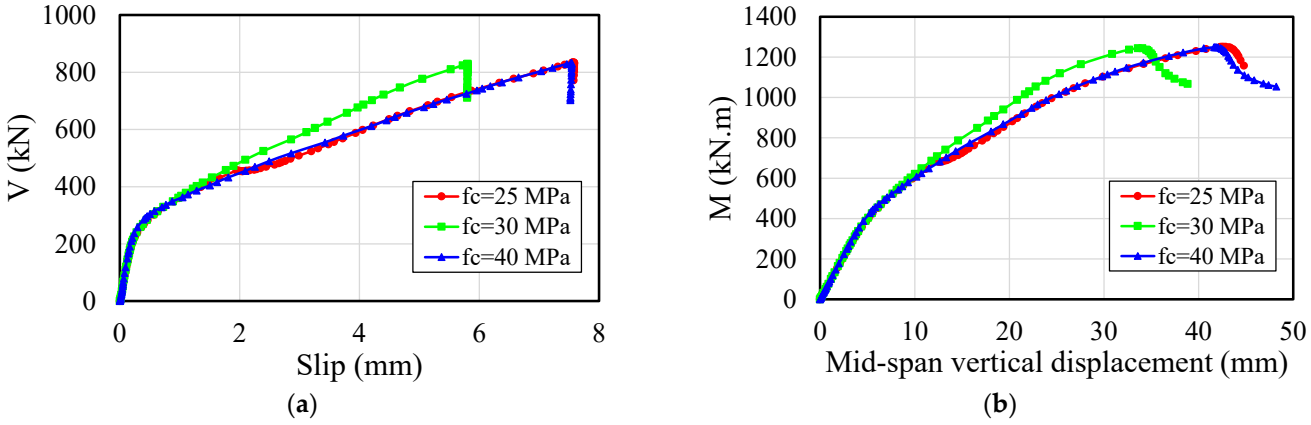

Figure 19. Influence of in situ concrete strength for the W460x74 section, φ = 16 mm and 225 mm of spacing: (**a**) shear-slip relationship; and (**b**) moment-deflection relationship.

These differences were observed for the concrete with the highest strength and transversal-reinforcement diameters equal to 12.5 mm and 16 mm. Figure 18 shows that the greater the concrete strength, the greater the initial stiffness of the composite beam, although the values for the ultimate moment were analogous, since the ultimate strength was governed by the slab. However, as the spacing between the connectors increased; that is, the interaction degree was reduced, as illustrated in Figure 19, the model with f_c = 30 MPa showed a different behavior in the shear-slip and moment-deflection relationships. This change in behavior was previously presented in Araújo et al. [20] and Ferreira et al. [25]. The authors reported that when the compressive strength of the in situ concrete was close to 40 MPa, the failure mode could occur in the shear stud, and for resistance values below 30 MPa, the failure could be governed by the in situ concrete.

Another important observation was that for models with 225 mm of spacing, considering the W460x51 section, the composite beams showed ductile behavior; that is, the slip at the steel–concrete interface was greater than 6 mm. Thus, it was possible to conclude that in all models analyzed for the W460x51 section and 225 mm of spacing, the behavior at the steel–concrete interface was characterized as ductile, according to prescriptions of Eurocode 4. For the f_c = 25 MPa models, the von Mises stresses in the shear studs, considering 175 mm and 225 mm of spacing, were greater than the models with 120 mm of spacing. A similar behavior occurred for f_c = 30 MPa models. For f_c = 40 MPa, there were models in which the von Mises stresses in the shear studs, considering 175 mm and 225 mm of spacings, were much higher than the models with 120 mm of spacing. This was observed for all transverse reinforcement diameters analyzed.

5.3. W530x72 Section

Considering 120 mm of spacing, for the midspan vertical displacement at 15 mm, the region where the composite beam was supported and the lower flange reached the yield resistance. The maximum von Mises stresses in the lower flange, web, and upper flange were 345 MPa, 316 MPa, and 230 MPa, respectively. When the composite beam reached the ultimate strength (Figure 20), for the midspan vertical displacement at 22 mm, the lower flange and approximately 1/4 of the web depth were in the plastic regime.

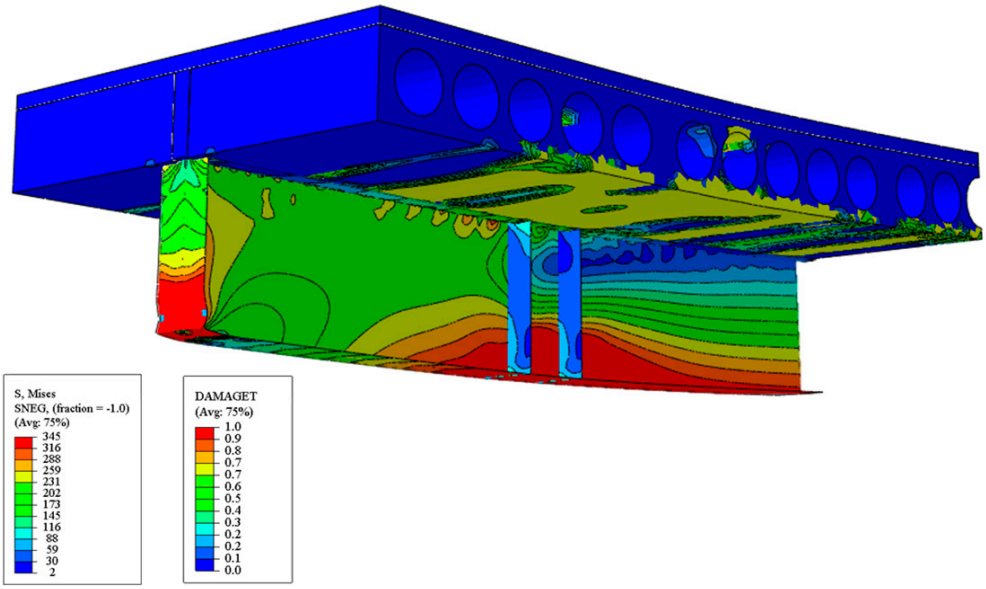

Figure 20. Final configuration for the W530x72 section, f_c = 40 MPa, φ = 16 mm, and 120 mm of spacing.

The ultimate strength was governed by excessive cracking of the slab. It is important to note that in these models, there were a better use of the steel section, in comparison with the previous cross-sections. This was due to the fact that the steel section had a depth and area greater than the other steel sections studied. So, the NPA tended to move in the direction of the steel section, a factor that favored the resistance of the hollow-core slab, thus reducing tension stresses. With the variation of the transverse reinforcement rate and in situ concrete strength, there were no differences in the shear-slip and moment-deflection relationships (similar to previous situations). Regarding the von Mises stresses in the shear studs, there were no significant differences, reaching values between 556 and 570 MPa.

On the other hand, considering 175 mm of spacing between the shear studs, for the midspan vertical displacement at 15 mm, only the support region reached the yield strength. The von Mises stresses in the lower flange, web, and upper flange were 316 MPa, 288 MPa, and 116 MPa, respectively. At the ultimate strength (Figure 21a), the midspan vertical displacement was 21 mm. In this loading stage, the lower flange was in the plastic regime.

For 225 mm of spacing, with the midspan vertical displacement at 15 mm, the results were similar to the previous beam. However, the maximum von Mises stresses in the lower flange, web, and upper flange were 288 MPa, 288 MPa, and 116 MPa, respectively. At the ultimate strength (Figure 21b), with the midspan vertical displacement at 38 mm, the lower flange, half the web depth, and the upper flange were in the plastic regime. With the variation of the transverse reinforcement rate and the in situ concrete strength, it was possible to verify some differences in the shear-slip and moment-deflection relationships (Figures 22 and 23).

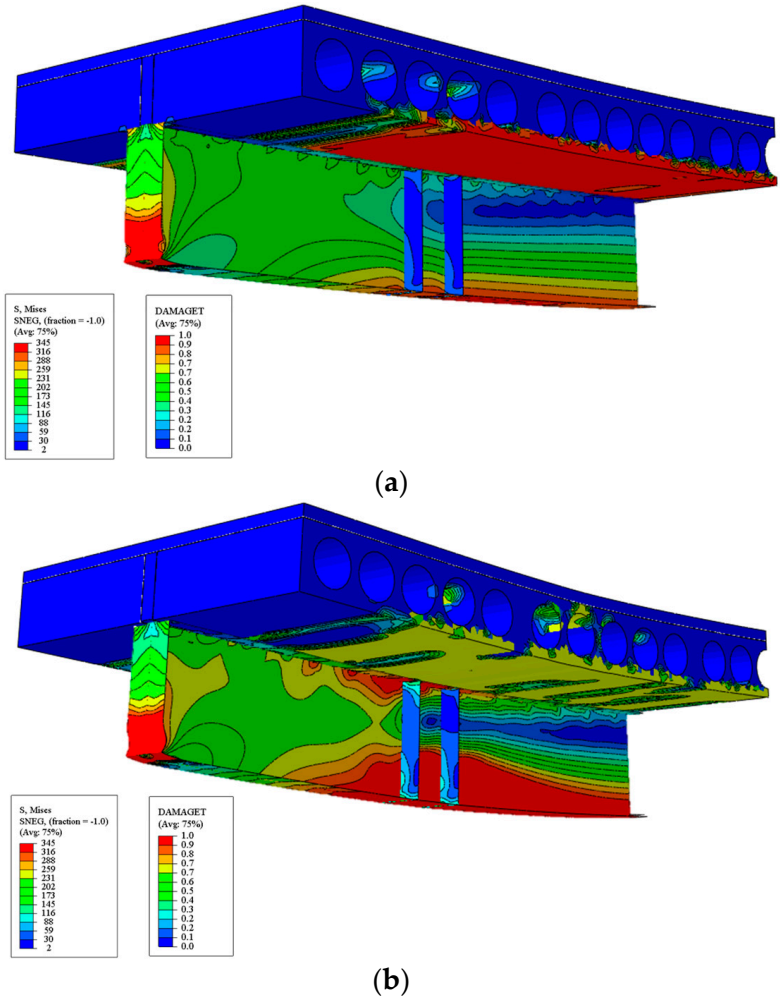

Figure 21. Final configuration for the W530x72 section: (**a**) 175 mm of spacing, f_c = 40 MPa, and φ = 16 mm; and (**b**) 225 mm of spacing, f_c = 40 MPa, and φ = 16 mm.

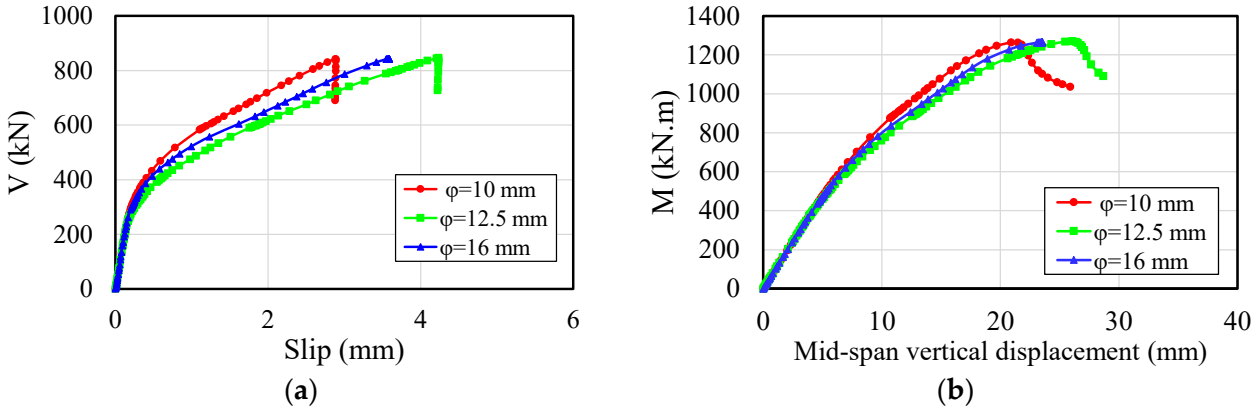

Figure 22. Influence of transverse reinforcement for the W530x72 section, f_c = 25 MPa and 175 mm of spacing: (**a**) shear-slip relationship; and (**b**) moment-deflection relationship.

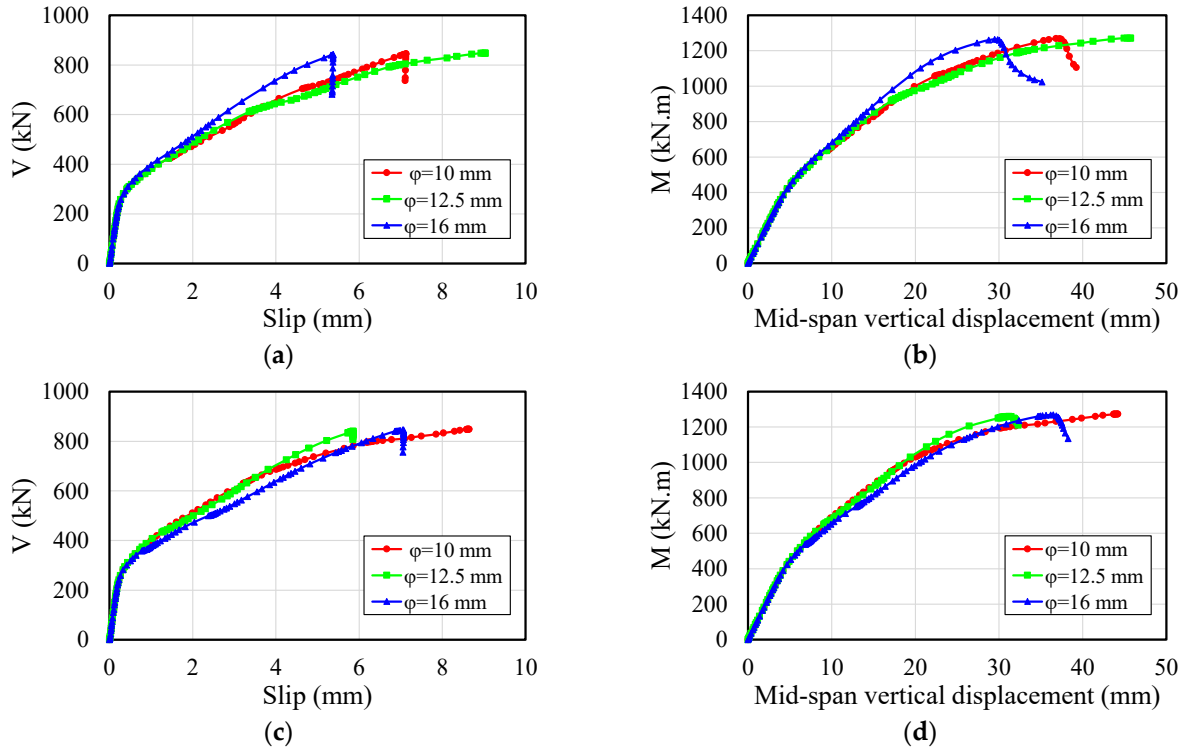

Figure 23. Influence of transverse reinforcement for the W530x72 section and 225 mm of spacing: (**a**) shear-slip relationship for f_c = 25 MPa; (**b**) moment-deflection relationship for f_c = 25 MPa; (**c**) shear-slip relationship for f_c = 30 MPa; and (**d**) moment-deflection relationship for f_c = 30 MPa.

It was observed that for the models with 175 mm of spacing, there were some differences in the relationships presented in Figure 22, considering a transverse reinforcement diameter of 12.5 mm and f_c = 25–30 MPa. On the other hand, for the models with 225 mm of spacing, these differences were observed (Figure 23) for a transverse reinforcement diameter of 16 mm and similar strength values for concrete. It is important to note that the behaviors shown in Figures 22 and 23 were similar to those presented in Figures 12 and 13.

5.4. Design

In this section, the results are presented in a summarized way, considering the ductile behavior (Figure 24), the maximum midspan vertical displacement for the service limit state for composite floors (Figure 25), and SCI P401 [19] procedure (Figure 26); and considering the strength models for shear studs presented in [19,20]. Considering full interaction and that NPA lies in the concrete slab (Equations (4)–(10)), in which A_a is the steel-section cross-sectional area, C_c is the concrete-flange axial strength, f_y is the steel-section yield strength, L is the composite-beam length, M_{pl} is the plastic moment of the composite section, Q_R is the shear-connector strength, t_c is overall depth of the concrete flange (including the concrete topping), T_a is the axial strength of the steel section in tension, and L_φ is the transverse reinforcement length.

$$\sum Q_R \geq A_a f_y \tag{4}$$

$$0.85 f_c b t_c \geq A_a f_y \tag{5}$$

$$C_c = 0.85 f_c b a \tag{6}$$

$$b \leq \begin{cases} L/4 \\ 2L_\phi + g \end{cases} \tag{7}$$

$$T_a = A_a f_y \tag{8}$$

$$a = \frac{T_a}{0.85 f_c b} \leq t_c \tag{9}$$

$$M_{pl} = T_a \left(\frac{d}{2} + t_c - \frac{a}{2} \right) \tag{10}$$

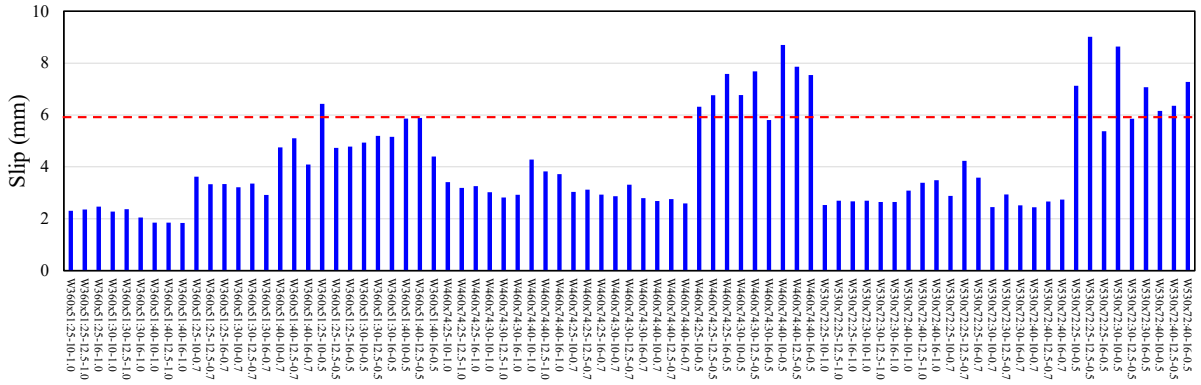

Figure 24. Maximum steel–concrete interface slips at ultimate behavior.

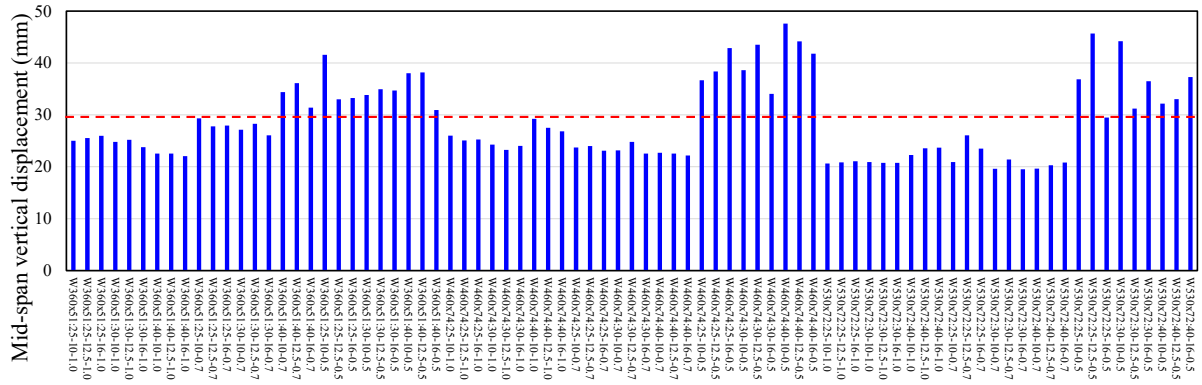

Figure 25. Maximum midspan vertical displacement at ultimate behavior.

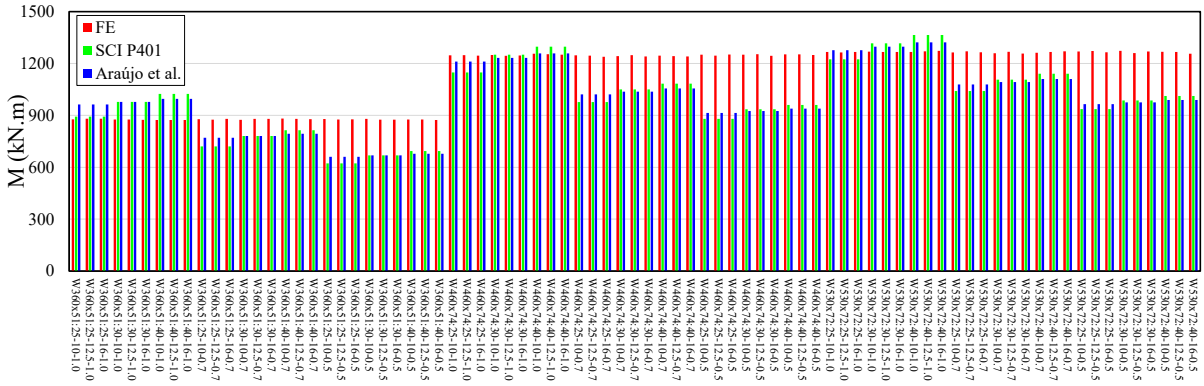

Figure 26. Comparison of finite element models vs. analytical procedures.

For partial interaction, the linear method was used, according to Eurocode 4 (Equation (11)), in which $M_{pl,a}$ is the plastic moment of the steel section, $M_{pl,FULL}$ is the plastic moment of the composite section with full shear connection, and η is the ratio of the sum of the strength of the shear studs provided to the sum of the strength of the shear studs needed for full shear connection.

$$M_{pl} = M_{pl,a} + \left(M_{pl,FULL} - M_{pl,a}\right)\eta \quad (11)$$

For a presentation of the results, a hypothesis of the minimum spacing was made; i.e., 120 mm providing full interaction. On the other hand, for the other spacings, partial interaction was considered. Therefore, for the spacings of 120 mm, 175 mm, 225 mm, the interaction degrees were 1.0, 0.7, and 0.5, respectively. As shown in Figure 24, only one situation for the W360 × 51 section presented a ductile behavior (f_c = 25 MPa, φ = 10 mm, and 225 mm of spacing). On the other hand, for all W460 × 74 and W530 × 72 models, considering 225 mm of spacing, ductile behavior was observed. This means that the greater the area of the steel cross-section and the greater the spacing between the shear studs, the greater the sliding in the steel–concrete interface. Respecting the midspan vertical displacement limit for floors ($L/200$), according to Eurocode 4, 52 observations were found below the limit value, specifically for all models of full interaction (Figure 25). Therefore, another observation was that the smaller the interaction degree, the greater the midspan vertical displacement. Finally, considering the calculation procedures mentioned in this section, a total of 60 observations were found in the conservative zone ($M_{FE} \leq M_{Rk}$). The observations that were shown to be unsafe ($M_{FE} > M_{Rk}$) were verified for models in which full interaction was considered (Figure 26).

5.5. Comparative Analyses

In this section, a comparison of the models developed in the present work was performed with those presented by Ferreira et al. [25] (Figure 27).

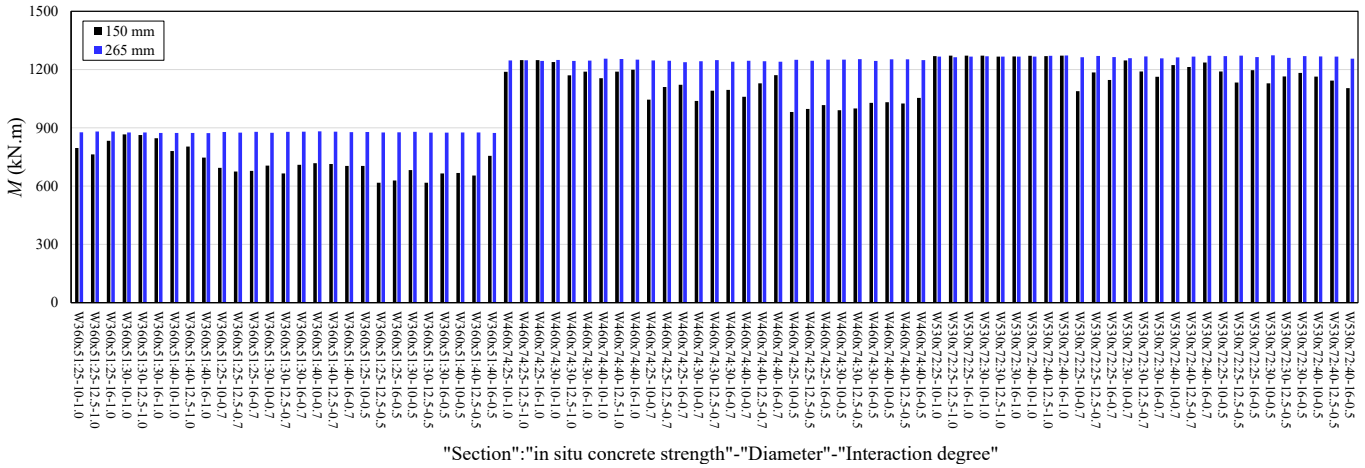

Figure 27. Comparative analyses between 150 mm and 265 mm PCHCS depth with concrete topping.

As noted, in some models, the higher PCHCS provided greater strength. This difference reached a maximum of 30%, considering the ratio of the 150 mm-depth PCHCS models to the 265 mm-depth PCHCS models. These values were measured considering the W360 × 51 section. With the increase in the steel cross-section (sections W460 × 74 and W530 × 72), this difference was not so significant. This demonstrated that for the models studied, it was not advantageous to increase the depth of the PCHCS, since the collapse was determined by the slab. In addition, the greater the depth of the hollow-core slab, the greater the weight of the structural system due to the higher consumption of concrete, and

thus the higher the costs. Therefore, from a sustainable and structural-efficiency point of view, the 150 mm depth PCHCS was the best option of the models studied.

6. Conclusions

Steel-Concrete composite beams with precast hollow-core slabs are a sustainable solution, and a better understanding of their parameters will yield more efficient designs. The present study developed a reliable finite element model to investigate some limitations imposed in the design recommendations of Steel-Concrete composite beams with precast hollow-core slabs, such as hollow-core-slab depth, transverse reinforcement rate, and shear-stud spacing. A parametric study was carried out, considering a 265 mm hollow-core unit with a concrete topping, since the SCI P401 recommendation is only applicable for 150–250 mm-deep hollow-core units. The parameters investigated were the in situ concrete strength, the transverse reinforcement rate, the interaction degree, and the steel cross-section. In total, 81 models were analyzed. The numerical results were compared with models of Steel-Concrete composite beams models, considering a 150 mm hollow-core unit with a concrete topping. In general, for the models that were considered under the partial-interaction hypothesis, there was a better efficiency of the structural system, providing greater deformations. Therefore, when designing Steel-Concrete composite beams with hollow-core slabs, considering partial interaction is a viable option, since it reduces the cost of the project, due to the smaller number of shear studs to be used, as well as the labor. Specifically, considering the parameters analyzed, it was concluded that:

1. In all models, the ultimate strength was reached by excessive cracking of the precast hollow-core slab. This occurred because the neutral plastic axis lay within the -core slab, a factor that generated tensile stresses. Thus, dimensioning Steel-Concrete composite beams with deeper hollow-core slabs is not advantageous. This is because the resistance is governed by the concrete slab, a factor that does not take advantage of the steel section. Therefore, in these analyzed models, there was a waste of material.
2. The greater the area of the steel cross-section, the greater the use of the steel section. When there is a larger steel cross-section, there is an increase in the plastic axial strength of the steel profile. This increase causes the neutral plastic axis to descend toward the steel profile, causing only compression stresses in the hollow-core slab.
3. The greater the spacing of the shear studs, the greater the use of the steel section. When considering the hypothesis of partial interaction, as presented for the models with 175 mm and 225 mm of spacing, the structural system can achieve ductile behavior, a factor that favors the ability of the structural elements to deform without reaching the ultimate strength. The use of a smaller number of shear connectors (175 mm and 225 mm models) provided resistance equivalent to the 120 mm models. Therefore, using a lower amount of material for the design of a structural system, as was the case with modeled Steel-Concrete composite beams, from the point of view of sustainability, there is a reduction in the embodied energy, since a smaller number of installed connectors will require a smaller amount of electricity consumption.
4. The transverse reinforcement rate had little influence on the ultimate strength of the models analyzed. This was because in most models, the fragile behavior was verified.
5. With the variation of the in situ concrete strength, there were no significant differences in the ultimate strength. Therefore, the use of lower in situ concrete strength can be advantageous; that is, the lower the concrete resistance, the greater the possibility that the plastic neutral axis will lie within the steel section. However, it is worth mentioning that the strength of concrete is also related to durability, a factor that certainly influences the life cycle of the structural element. The greater the durability of the structural system, the less the need for excessive maintenance, thus contributing to the reduction of waste and embodied energy.
6. Ductile behavior was observed for models with 225 mm of spacing, considering the W460 $\times$ 74 and W530 $\times$ 72 sections. It also was verified that the lower the interaction

degree, the greater the midspan vertical displacement, which may exceed the limit of $L/200$.

7. Regarding the verification of strength with the calculation procedure, some models that considered full interaction proved to be unsafe ($M_{FE} \leq M_{Rk}$). On the other hand, all observations considering partial interaction proved to be safe ($M_{FE} > M_{Rk}$).
8. The numerical models with a 265 mm hollow-core unit presented greater resistance than the models with a150 mm hollow-core unit, considering the W360 × 51 section. However, for the W460 × 74 and W530 × 72 sections, there were no significant differences. The basic difference between the models compared was 115 mm of precast concrete. Therefore, for the numerical models evaluated, using a smaller amount of precast concrete provided a better efficiency of the structural system. The use of a lower volume of concrete in a structural project provides a reduction in the structure's own weight, and in terms of sustainability, a lower amount of CO_2 emissions.

Author Contributions: Conceptualization, F.P.V.F. and K.D.T.; methodology, F.P.V.F., K.D.T. and S.D.N.; software, F.P.V.F.; validation, F.P.V.F.; investigation, F.P.V.F.; writing—original draft preparation, F.P.V.F., K.D.T., C.H.M. and S.D.N.; writing—review and editing, F.P.V.F., K.D.T., C.H.M. and S.D.N.; visualization, K.D.T., C.H.M. and S.D.N.; supervision, S.D.N.; project administration, S.D.N.; funding acquisition, F.P.V.F. All authors have read and agreed to the published version of the manuscript.

Funding: This research was funded by the São Paulo Research Foundation (FAPESP) (grant number #2018/22803-1).

Acknowledgments: The authors would like to thank Construção Metálica—Gerdau Aços Brasil for making available the data related to COPPETEC, PEC-18541.

Conflicts of Interest: The authors declare no conflict of interest.

References

1. Cabeza, L.F.; Boquera, L.; Chàfer, M.; Vérez, D. Embodied energy and embodied carbon of structural building materials: Worldwide progress and barriers through literature map analysis. *Energy Build.* **2021**, *231*, 110612. [CrossRef]
2. Whitworth, A.H.; Tsavdaridis, K.D. Genetic algorithm for embodied energy optimisation of steel-concrete composite beams. *Sustainability* **2020**, *12*, 3102. [CrossRef]
3. Whitworth, A.; Tsavdaridis, K. Embodied energy optimization of steel-concrete composite beams using a genetic algorithm. *Procedia Manuf.* **2020**, *44*, 417–424. [CrossRef]
4. European Committee for Standardization. *EN 1994-1-1: Eurocode 4—Design of Composite Steel and Concrete Structures—Part 1-1: General Rules for Buildings*; European Committee for Standardization: Brussels, Belgium, 2004.
5. Ibrahim, I.; Elliott, K.; Abdullah, R.; Kueh, A.; Sarbini, N. Experimental study on the shear behaviour of precast concrete hollow core slabs with concrete topping. *Eng. Struct.* **2016**, *125*, 80–90. [CrossRef]
6. Baran, E. Effects of cast-in-place concrete topping on flexural response of precast concrete hollow-core slabs. *Eng. Struct.* **2015**, *98*, 109–117. [CrossRef]
7. Girhammar, U.A.; Pajari, M. Tests and analysis on shear strength of composite slabs of hollow core units and concrete topping. *Constr. Build. Mater.* **2008**, *22*, 1708–1722. [CrossRef]
8. Araújo, D.D.L.; Sales, M.W.R.; Silva, R.P.M.; Antunes, C.D.F.M.; Ferreira, M.D.A. Shear strength of prestressed 160 mm deep hollow core slabs. *Eng. Struct.* **2020**, *218*, 110723. [CrossRef]
9. Albero, V.; Saura, H.; Hospitaler, A.; Montalvà, J.; Romero, M.L. Optimal design of prestressed concrete hollow core slabs taking into account its fire resistance. *Adv. Eng. Softw.* **2018**, *122*, 81–92. [CrossRef]
10. De Nardin, S.; El Debs, A.L. State of the art of Steel-Concrete composite structures in Brazil. *Proc. Inst. Civ. Eng. Civ. Eng.* **2013**, *166*, 20–27. [CrossRef]
11. Lam, D. Capacities of headed stud shear connectors in composite steel beams with precast hollowcore slabs. *J. Constr. Steel Res.* **2007**, *63*, 1160–1174. [CrossRef]
12. Tawadrous, R.; Morcous, G. Shear strength of deep hollow-core slabs. *ACI Struct. J.* **2018**, *115*, 699–709. [CrossRef]
13. Ahmed, K.E.-S.; Abdulrahman, M.; Alhozaimy, A.M. Web shear resistance of prestressed precast deep hollow core slabs. *Struct. J.* **2016**, *116*, 139–150. [CrossRef]
14. De Souza, P.T.; Kataoka, M.N.; El Debs, A.L.H. Experimental and numerical analysis of the push-out test on shear studs in hollow core slabs. *Eng. Struct.* **2017**, *147*, 398–409. [CrossRef]

15. Ahmed, I.M.; Tsavdaridis, K.D. Life cycle assessment (LCA) and cost (LCC) studies of lightweight composite flooring systems. *J. Build. Eng.* **2018**, *20*, 624–633. [CrossRef]
16. Dong, Y.H.; Jaillon, L.; Chu, P.; Poon, C. Comparing carbon emissions of precast and cast-in-situ construction methods—A case study of high-rise private building. *Constr. Build. Mater.* **2015**, *99*, 39–53. [CrossRef]
17. Lam, D. Composite Steel Beams Using Precast Concrete Hollow Core Floor Slabs. 1998. Ph.D. Thesis, University of Nottingham, Nottingham, UK, 1998.
18. Batista, E.M.; Landesmann, A. Análise experimental de vigas mistas de aço e concreto compostas por lajes alveolares e perfis laminados. COPPETEC, PEC-18541 2016. Unpublished.
19. Gouchman, G.H. *Design of Composite Beams Using Precast Concrete Slabs in Accordance with EUROCODE 4*; The Steel Construction Institute: London, UK, 2014.
20. Araújo, D.D.L.; Sales, M.W.R.; de Paulo, S.M.; de Cresce El, A.L. Headed steel stud connectors for composite steel beams with precast hollow-core slabs with structural topping. *Eng. Struct.* **2016**, *107*, 135–150. [CrossRef]
21. Lam, D.; Elliott, K.S.; Nethercot, D.A. Experiments on composite steel beams with precast concrete hollow core floor slabs. *Proc. Inst. Civ. Eng. Struct. Build.* **2000**, *140*, 127–138. [CrossRef]
22. Lam, D.; Elliott, K.; Nethercot, D. Parametric study on composite steel beams with precast concrete hollow core floor slabs. *J. Constr. Steel Res.* **2000**, *54*, 283–304. [CrossRef]
23. El-Lobody, E.; Lam, D. Modelling of headed stud in steel-precast composite beams. *Steel Compos. Struct.* **2002**, *2*, 355–378. [CrossRef]
24. Hicks, S.J.; Lawson, R.M. *Design of Composite Beams Using Precast Concrete Slabs*; The Steel Construction Institute: London, UK, 2003.
25. Ferreira, F.P.V.; Martins, C.H.; De Nardin, S. A parametric study of steel-concrete composite beams with hollow core slabs and concrete topping. *Structures* **2020**, *28*, 276–296. [CrossRef]
26. Ferreira, F.P.V.; Martins, C.H.; De Nardin, S. Advances in composite beams with web openings and composite cellular beams. *J. Constr. Steel Res.* **2020**, *172*, 106182. [CrossRef]
27. Walraven, J.C.; Mercx, W.P.M. The bearing capacity of prestressed hollow core slabs. *Heron* **1983**, *28*, 1–46.
28. Nguyen, T.H.; Tan, K.-H.; Kanda, T. Investigations on web-shear behavior of deep precast, prestressed concrete hollow core slabs. *Eng. Struct.* **2019**, *183*, 579–593. [CrossRef]
29. Joo, H.-E.; Han, S.-J.; Park, M.-K.; Kim, K.S. Shear tests of deep hollow core slabs strengthened by core-filling. *Appl. Sci.* **2020**, *10*, 1709. [CrossRef]
30. Michelini, E.; Bernardi, P.; Cerioni, R.; Belletti, B. Experimental and numerical assessment of flexural and shear behavior of precast prestressed deep hollow-core slabs. *Int. J. Concr. Struct. Mater.* **2020**, *14*, 1–17. [CrossRef]
31. Brunesi, E.; Bolognini, D.; Nascimbene, R. Evaluation of the shear capacity of precast-prestressed hollow core slabs: Numerical and experimental comparisons. *Mater. Struct.* **2014**, *48*, 1503–1521. [CrossRef]
32. Palmer, K.D.; Schultz, A.E. Experimental investigation of the web-shear strength of deep hollow-core units. *PCI J.* **2011**, *56*, 83–104. [CrossRef]
33. ABAQUS 6.18 (2016) FEA computer software, Version 6.12, Product.
34. Ferreira, F.P.V.; Rossi, A.; Martins, C.H. Lateral-torsional buckling of cellular beams according to the possible updating of EC3. *J. Constr. Steel Res.* **2019**, *153*, 222–242. [CrossRef]
35. Ferreira, F.P.V.; Martins, C.H. LRFD for lateral-torsional buckling resistance of cellular beams. *Int. J. Civ. Eng.* **2019**, *18*, 303–323. [CrossRef]
36. Rossi, A.; Ferreira, F.P.V.; Martins, C.H.; Júnior, E.C.M. Assessment of lateral distortional buckling resistance in welded I-beams. *J. Constr. Steel Res.* **2020**, *166*, 105924. [CrossRef]
37. Ferreira, F.P.V.; Martins, C.H.; De Nardin, S. Assessment of web post buckling resistance in steel-concrete composite cellular beams. *Thin-Walled Struct.* **2021**, *158*, 106969. [CrossRef]
38. Ferreira, F.P.V.; Martins, C.H.; De Nardin, S. Sensitivity analysis of composite cellular beams to constitutive material models and concrete fracture. *Int. J. Struct. Stab. Dyn.* **2021**, *21*, 2150008. [CrossRef]
39. Ferreira, F.P.V.; Tsavdaridis, K.D.; Martins, C.H.; De Nardin, S. Buckling and post-buckling analyses of composite cellular beams. *Compos. Struct.* **2021**, *262*, 113616. [CrossRef]
40. Ferreira, F.P.V.; Tsavdaridis, K.D.; Martins, C.H.; De Nardin, S. Ultimate strength prediction of Steel-Concrete composite cellular beams with PCHCS. *Eng. Struct.* **2021**, *236*, 112082. [CrossRef]
41. Chen, S.; Jia, Y. Numerical investigation of inelastic buckling of Steel-Concrete composite beams prestressed with external tendons. *Thin-Walled Struct.* **2010**, *48*, 233–242. [CrossRef]
42. Zhou, W.-B.; Yan, W.-J. Refined nonlinear finite element modelling towards ultimate bending moment calculation for concrete composite beams under negative moment. *Thin-Walled Struct.* **2017**, *116*, 201–211. [CrossRef]
43. El-Lobody, E.; Lam, D. Finite element analysis of steel-concrete composite girders. *Adv. Struct. Eng.* **2003**, *6*, 267–281. [CrossRef]
44. Hillerborg, A.; Modéer, M.; Petersson, P.-E. Analysis of crack formation and crack growth in concrete by means of fracture mechanics and finite elements. *Cem. Concr. Res.* **1976**, *6*, 773–781. [CrossRef]
45. Lubliner, J.; Oliver, J.; Oller, S.; Oñate, E. A plastic-damage model for concrete. *Int. J. Solids Struct.* **1989**, *25*, 299–326. [CrossRef]
46. Lee, J.; Fenves, G.L. Plastic-damage model for cyclic loading of concrete structures. *J. Eng. Mech.* **1998**, *124*, 892–900. [CrossRef]

47. Genikomsou, A.S.; Polak, M.A. Finite element analysis of punching shear of concrete slabs using damaged plasticity model in ABAQUS. *Eng. Struct.* **2015**, *98*, 38–48. [CrossRef]
48. Duvaut, G.; Lions, J.L. *Inequalities in Mechanics and Physics*; Springer: Berlin/Heidelberg, Germany, 1976; Volume 219.
49. Behnam, H.; Kuang, J.; Samali, B. Parametric finite element analysis of RC wide beam-column connections. *Comput. Struct.* **2018**, *205*, 28–44. [CrossRef]
50. Stress-strain relationship for plain concrete in compression. *ACI J. Proc.* **1985**, *82*, 797–804. [CrossRef]
51. Carreira, D.J.; Chu, K.H. Stress-strain relatonship for reinforced concrete in tension. *J. Am. Concr. Inst.* **1986**, *83*, 21–28.
52. Pathirana, S.W.; Uy, B.; Mirza, O.; Zhu, X. Flexural behaviour of composite steel–concrete beams utilising blind bolt shear connectors. *Eng. Struct.* **2016**, *114*, 181–194. [CrossRef]
53. Liu, X.; Bradford, M.A.; Chen, Q.-J.; Ban, H. Finite element modelling of Steel-Concrete composite beams with high-strength friction-grip bolt shear connectors. *Finite Elem. Anal. Des.* **2016**, *108*, 54–65. [CrossRef]
54. Sjaarda, M.; Porter, T.; West, J.S.; Walbridge, S. Fatigue behavior of welded shear studs in precast composite beams. *J. Bridge Eng.* **2017**, *22*, 04017089. [CrossRef]
55. Guezouli, S.; Lachal, A. Numerical analysis of frictional contact effects in push-out tests. *Eng. Struct.* **2012**, *40*, 39–50. [CrossRef]
56. Crisfield, M. A fast incremental/iterative solution procedure that handles "snap-through". *Comput. Struct.* **1981**, *13*, 55–62. [CrossRef]
57. Crisfield, M.A. Snap-through and snap-back response in concrete structures and the dangers of under-integration. *Int. J. Numer. Methods Eng.* **1986**, *22*, 751–767. [CrossRef]
58. Maewal, A.; Nachbar, W. Stable postbuckling equilibria of axially compressed, elastic circular cylindrical shells: A finite-element analysis and comparison with experiments. *J. Appl. Mech.* **1977**, *44*, 475–481. [CrossRef]